REAL-TIME PLASMA DENSITY CONTROL VIA A MODIFIED HOLLOW-CATHODE PLASMA SOURCE WITH A VARIABLE APERTURE

Jesse K. McTernan,[(1)] Sven G. Bilén,[(1)] and John D. Williams[(2)]

[(1)]The Pennsylvania State University, 213 Hammond Bldg., University Park, PA 16801, USA, jkm249@psu.edu
[(2)]Colorado State University, Fort Collins, CO 80523, USA

ABSTRACT

We modified a plasma source used in ground-based simulations of the low-Earth-orbit environment. This modification allows for real-time control of ion and electron densities with minimal impact on the other plasma parameters. Specifically, we modified the output grid (i.e., aperture) to range from fully closed (0%) to fully open (100%). In the range of 4% to 100%, the ion and electron densities changed from 0.2×10^{13} m^{-3} to 2.2×10^{13} m^{-3}. In this range, the electron temperature, plasma potential, and floating potential remained nearly constant. System settling time was on the order of 10s of seconds after a 10% adjustment was made to the aperture.

1. INTRODUCTION

Spacecraft in low Earth orbit (LEO) experience streaming ions (~5 eV) and thermal electrons (~0.1 eV) since the velocity of the spacecraft is greater than the thermal velocity of the ions yet less than the thermal velocity of the electrons. This is called the mesothermal condition. The result is an asymmetry of particle fluxes onto the outer surfaces of a spacecraft. Ions tend to interact or collide with the ram surfaces, whereas electrons could potentially interact with all outer surfaces.

There have been attempts to reproduce the mesothermal condition in ground-based vacuum facilities in order to study HV solar arrays in LEO [1], current collection [2], material interactions with the LEO environment [3], and to create a testbed for plasma diagnostic equipment before being used in the space environment [4]. As indicated in [4], many of these attempts compromised the fidelity of the plasma environment by either obtaining high-energy streaming ions or low-energy electrons, but not both simultaneously.

Reference [4] developed a magnetic filter–type plasma source ("the source") capable of simultaneously producing streaming ions with energies over the range of 1–4 eV and thermal electrons with energies ranging from 0.17–0.35 eV—in good agreement with the LEO environment. The filtering is achieved by a ring-cusp magnetic field that confines high-energy electrons, yet permits streaming ions to "leak" out of the source. Low-energy electrons are pulled along with the ions. The theory of operation of the plasma source and a comparison to other similar plasma sources is presented in their paper. The plasma source can be configured to operate using argon, nitrogen, hydrogen, krypton, and xenon. Reference [6] configured the source to operate on atomic oxygen.

In this paper, we describe a modification to the aforementioned plasma source that enables real-time adjustment to the electron and ion density with minimal impact on the other plasma parameters. We achieved this by modifying the grid of the plasma source such that the effective output aperture can be controlled using an overlapping grid system actuated by a stepper motor (Fig. 1).

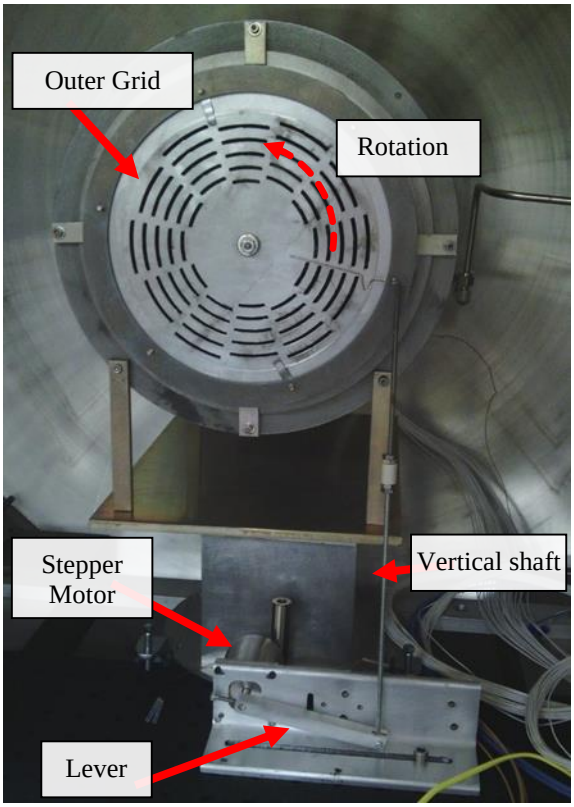

Figure 1. Adjustable grid attached to plasma source and installed in vacuum chamber. Here, the grid is fully open. A stepper motor is located beneath the source. The lever moves a vertical shaft, which rotates the outer grid to change the open area of the source.

This paper is organized as follows. Section 2 describes the system and procedures used including the vacuum facilities and diagnostic equipment. In Section 3, we describe the modification to the plasma source. Next, we discuss the results of the modification and the effect on the plasma environment in Section 4. Section 5 concludes with some discussion and suggestions for future work. Figure

2. SYSTEM SETUP AND PROCEDURES

Fig. 2 shows a schematic of our simulation system. We use a cylindrical vacuum chamber (Lesker Company) that is approximately 40 inches (102 cm) in length and 35 inches (89 cm) in diameter. Taking into account the feed-through ports, windows, and internal structures, the internal volume is approximately 24.4 ft^3 (0.69 m^3). A CTI-Cryogenics Cryo-Torr 7 high-vacuum pump and an Edwards EXT255H turbo pump can produce a base pressure of 1.6×10^{-5} Torr. A viewport allows visual confirmation of the creation of a plasma inside the plasma source. Refer to [5] for more details.

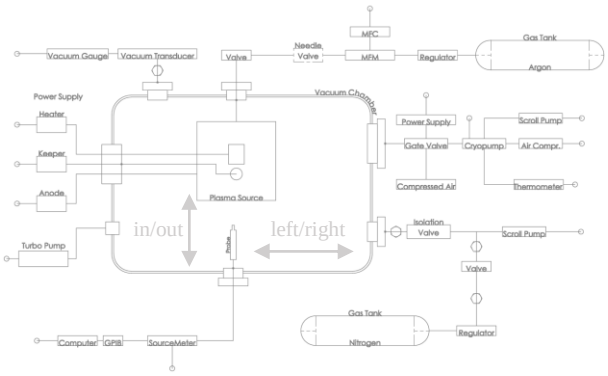

Figure 2. System Schematic. See a digital copy of this paper to zoom in for details.

The gas feed system consists of an ultra-high purity regulator (Harris), 0–10 sccm mass flow controller (MKS), and a flow controller bypass that creates a low conductance path from the vacuum chamber to the regulator. We currently use argon (99.999% pure) as the ionizing gas. The flow rate for all experiments was 3.5 sccm, which created an operating background pressure of 1.3×10^{-4} Torr. This corresponds to atmospheric pressure at about 110 km altitude.

Preliminary mapping of the plasma in the horizontal plane and coincident with the center of the source reveals that the plasma is very uniform in a plane *perpendicular* to the cylindrical axis of the source and mostly uniform in a plane *along* the cylindrical axis of the source. In other words, there is hardly any variation in the "left/right" direction and only some change "in/out" (Fig. 2). An object moved toward the source by as much as 10 cm (4 inches) will experience effectively the same plasma potential and electron temperature. The electron density will increase from 6.4×10^{12} m^{-3} to 8.4×10^{12} m^{-3}.

The plasma diagnostics tools were a cylindrical Langmuir probe (LP) and a three-grid retarding potential analyzer (RPA). The LP was manufactured from 0.011-in-diameter (0.028 cm) stainless steel rod 2.5 in (6.4 cm) in length. A probe of these dimensions satisfies the orbital-motion-limited (OML) condition described by [7] since the radius is smaller than the Debye length and the aspect ratio (i.e., length/radius) is >> 1. Long, thin probes approximate an infinite cylinder with minimal distortion from edge effects. Data from the LP corresponded well with OML theory.

We used an RPA (i.e., Faraday cup) from Kimball Physics (model FC-71), which has three grids (ground, retarding, and suppression) listed in the order in which a charged particle encounters them. The ground grid was held at the chamber ground. The retarding grid was biased to −20 V to prevent electrons from entering the RPA. Finally, the suppression grid was swept from 0 V to +10 V, while measuring the current to the collector, which was biased to −100 V. The derivative of the current with respect to the voltage is proportional to the ion energy [8]. The aperture of the grids was 5.0 mm. The collector had an area of 2.54 cm^2.

The plasma diagnostic equipment was positioned 0.5 m downstream of the source. The mean free path of the argon charge-exchange (CEX) ions was greater than this distance. We calculated the CEX mean free path based on the methods proposed by [9], [10], and [11], which yielded 0.863 m, 0.662 m, and 0.637 m, respectively. CEX ions are low energy ions resulting from a collision of a high energy argon ion with a neutral argon atom. The energies of the resulting CEX ions are close to the plasma potential and are undesirable. The kinetic energy is, instead, given to the neutral atom, which has no value in this context.

Table 1 displays a comparison of our research facilities with the facilities where the plasma source was developed and initially evaluated [4]. The vacuum pumping equipment used in the work of [4] produced a lower pressure than what we were capable of producing. This restricted our flow rates to lower values, otherwise CEX ions would dominate. A plot of the chamber pressure vs. flow rate is shown in Fig. 3.

Table 1. Comparison between the conditions at our research facilities and where the source was developed.

	This work	Ref. [4]
Base pressure [$\times10^{-5}$ Torr]	1.6	0.2
Gas	Argon	Argon
Flow rate [sccm]	3.5	1–15
Operating pressure [$\times10^{-5}$ Torr]	13	1–10
Diagnostics dist. from source [m]	0.5	0.5
Diagnostic tools	RPA/LP	RPA/LP

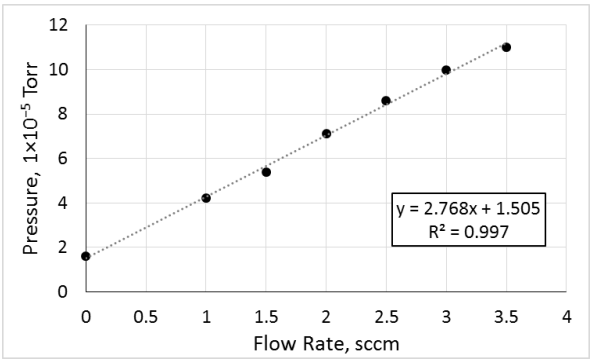

Figure. 3. Plot of chamber pressure versus flow rate.

3. MODIFICATION OF THE PLASMA SOURCE

The plasma source has stainless steel grids (or screens) at the output that are used to increase the impedance seen by the neutral atoms. This increases the residence time of the neutrals within the source and increases the chance of ionization [4]. The area of the "open" sections (i.e., the aperture) of the grid also affects the plasma density exiting the source. We modified the grids to have an adjustable aperture that varies from fully open to fully closed in approximately 115 increments. The increments are only limited by the mechanisms that close the aperture, in our case a stepper motor with microstepping enabled.

The basic operation consists of two concentric grid parts (Fig. 4) that have alternate hole patterns. When the smaller (outer) grid rotates the hole size (aperture) can be increased or decreased. This also increases or decreases the effective transparency of the grid to the plasma.

There is a stainless steel rod spot welded to the outer grid (Fig. 5) that is connected to a vertical shaft. The vertical shaft is attached to a lever, which is connected to a stepper motor (Figs. 1 and 6). The motor is controlled external to the chamber. The axis of rotation of the grid and the axis of rotation of the motor are aligned. The vertical distance between the two axes is equal to the vertical shaft length. The distance from the rotation axes to the connection points on the shaft is equal to the lever length. Therefore, a change in angle of the stepper motor equals the change in angle of the outer grid (Fig. 6).

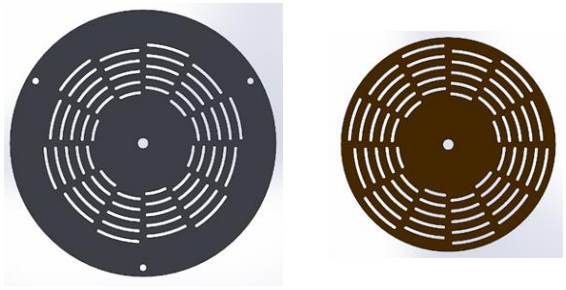

a. *b.*

Figure 4. Adjustable grid with a) an inner, larger part and b) an outer, smaller part. The outer part is free to rotate around its center, which is concentric with the inner part.

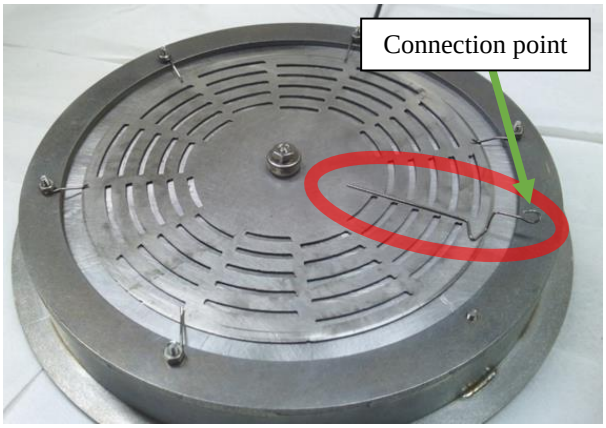

Figure 5. A stainless steel rod (circled in red) was shaped and then spot welded to the outer grid. It connects to the vertical shaft at the connection point indicated.

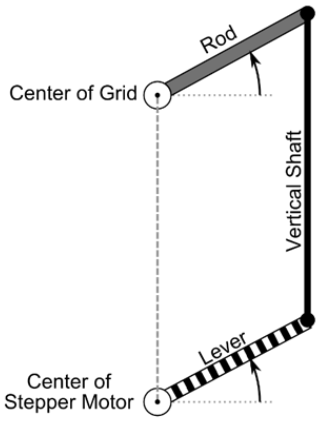

Figure 6. The distance from the center of the grid and center of stepper motor equals the length of the vertical shaft. The length of the lever is equal to the length of the connection rod. Therefore, a change in angle of the stepper motor is commensurate with a change in angle of the outer grid.

The original design of the grid and magnet assembly used a friction fit to tightly hold the magnet assembly against the grid. However, when using an adjustable grid, the outer part needs to rotate freely and cannot be used as structural support. Therefore, we added two ceramic spacers to the magnet assembly to keep the assembly parallel to the grid. First, we spot welded a stainless steel bolt, then inserted a ceramic standoff. The two standoffs and the center bolt form a tripod shape that supports the magnet assembly while keeping it electrically isolated (Fig. 7).

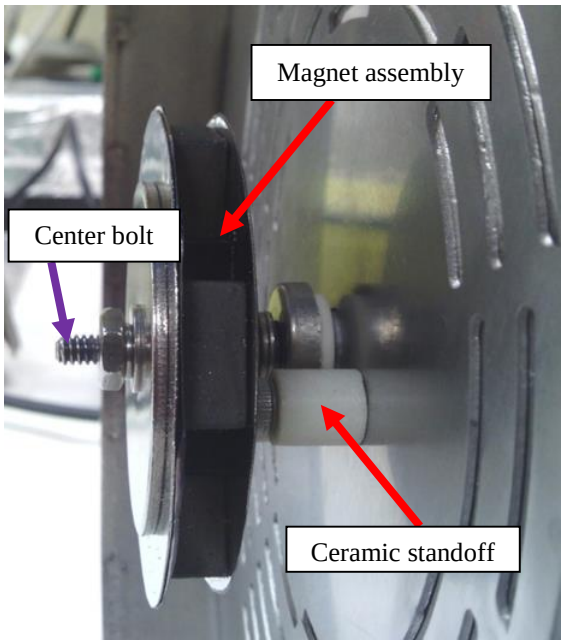

Figure 7. Two ceramic standoffs (one not seen) and a central bolt form a tripod shape that supports the magnet assembly and keeps it level to the grid (while maintaining electrical isolation from the grid).

To keep the outer grid against the inner gird, five stainless steel "fingers" applied gentle pressure to the outer grid (Figs. 5 and 8). A previous design (shown in Fig. 1) used two stainless steel tabs. But, when the plasma was on, the grid would bind (i.e., jam). It is assumed that the grids expanded due to the heat; a significant lesson learned. We found that even the finger system would bind when the anode operated >325 W.

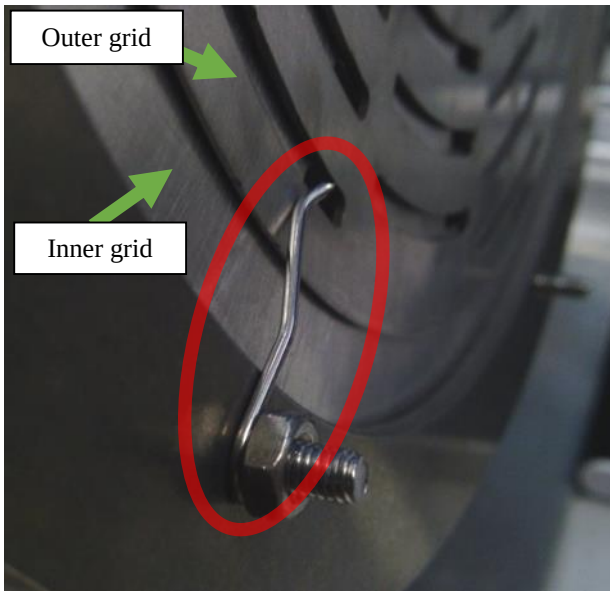

Figure 8. Stainless steel "fingers" (circled in red) apply a force to the outer grid to keep it against the inner grid. The applied pressure is light, otherwise the grid will bind due to thermal expansion.

The adjustable grid has been successfully working for over 60 hours of plasma source operation including 14 on/off cycles, which produced thermal stresses and strains.

4. RESULTS AND DISCUSSION

The largest aperture of our adjustable grid is, by design, half the aperture of the original grid. Typical electron temperatures and densities using the original design were approximately 0.15 eV and 8×10^{12} m^{-3} (keeper at 1.5 A, heater at 4.0 A, anode at 2.0 A, flow at 3.5 sccm, and pressure approximately 1.2×10^{-4} Torr). The resulting densities using the modified grid at similar conditions were, as expected, about half.

We then measured the plasma parameters as a function of aperture opening (where 100% was fully open). For the remainder of the experiments, the anode current was increased to 10 A to get higher streaming ion energies. The system settled approximately 2 minutes after making aperture adjustments, confirmed by changes in floating potential of a conductive object in the plasma, settling of power supplies, and repeatability of data collection. The majority of the settling occurred with 10s of seconds of a 10% aperture change.

As seen in Fig. 9, the change in electron and ion densities as a function of aperture opening was approximately linear from aperture openings from 20% to 100%. There was little change in the electron temperature, plasma potential, and floating potential within the same range. In the full range, the plasma density changed from 0.07×10^{13} m^{-3} to 2.2×10^{13} m^{-3}.

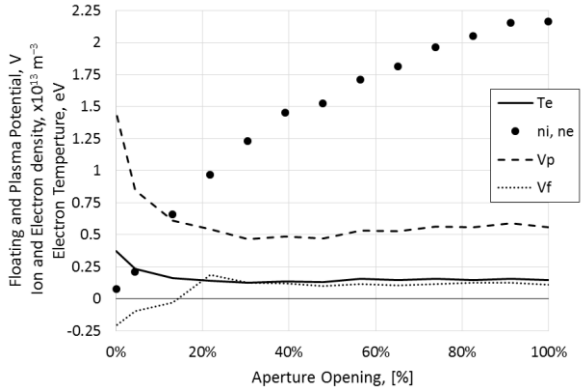

Figure 9. Plasma parameters as a function of aperture opening. In the range of 20% to 100%, the change in electron and ion densities is nearly linear while electron temperature is constant.

We analyzed the data and derived the plasma parameters using the method described in [12]. We intended to use the RPA to measure the ion energies and use those values in place of the velocity of the International Space Station, found in Eq. 7 [12]. However, our RPA measurements were inconclusive.

Instead, we performed a nonlinear least-squares fit like in [12] leaving ion energy as a variable. We found a value of ion energy that yielded ion densities equal to electron densities, that is, we assumed quasi-neutrality in the chamber. A representative plot showing the non-linear fit is shown in Fig. 10. Excellent agreement is seen between the data and the fit.

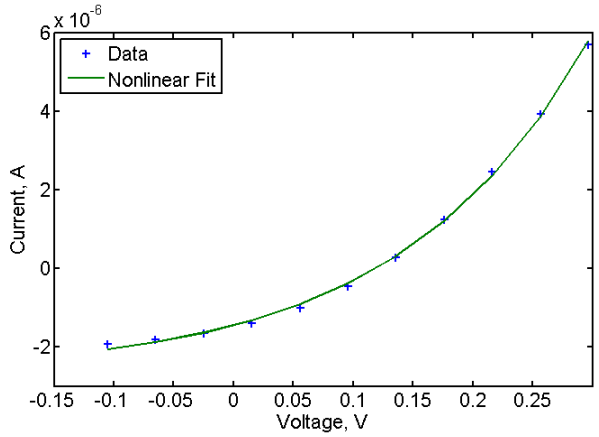

Figure 10. This is a representative plot showing good agreement between the fit (green line) and the raw data (blue plus signs). We performed a non-linear least squares fit based on the method in [12].

Fig. 11 shows the resulting ion energy that yielded an ion density equal to electron density in the data-fit model. It appears that the ion energy increased from approximately 7 eV to 14 eV in the range of aperture opening from 100% to 20%. We intend to solve our issues with the RPA to corroborate calculated ion energies with measured energies. It is interesting to note that the streaming ion energy approaches zero when the grid is fully closed, as expected. This gives some confidence that the data fit model properly accounts for ion energies. Nonetheless, the calculated values of ion energies as large as 14 eV are not likely since previous research indicates streaming ions of approximately 5 eV.

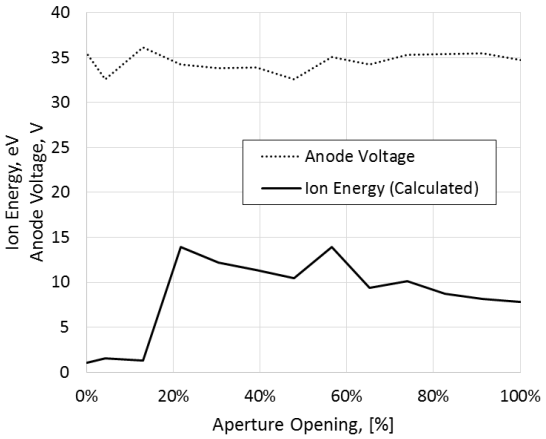

Figure 11. We adjusted the ion energy in the data fit model until ion density equaled the electron density (thus assuming quasi-neutrality). This was necessary since our RPA measurements were inconclusive.

The outer grid showed significant signs of heating (Fig. 12). The outer grid can be exposed to over 500 W of electrical power when the anode is operating at 10 A at 50 V. At low flow rates (approximately 1–3 sccm), the anode voltage was over 45 V. Higher flow rates (>3.5 sccm) will lower the anode voltage, but increase the chamber pressure. Therefore, a balance between anode voltage and pressure is needed based on the user's equipment.

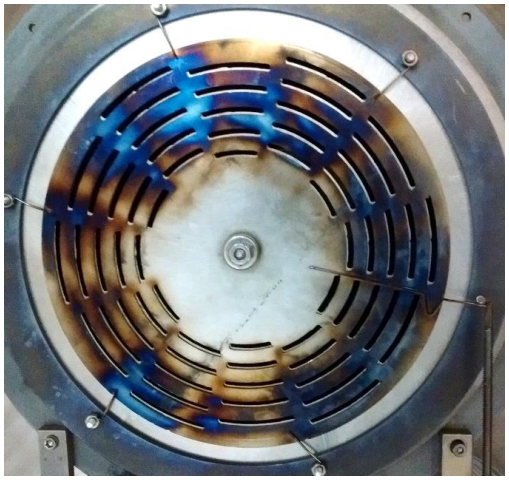

Figure 12. The outer grid experienced significant heating. Compare this image with Figs. 1 and 5.

The only thermal connection the outer grid had was at the "fingers" seen in Figs. 5, 8, and 12, leaving radiative cooling as the dominant heat loss mechanism. We suspect that this is why only the outer grid appears to show signs of significant heating. As mentioned in Sec. 3, the grid would bind when the anode power was greater than 325 W. The grid would return to normal operation when given sufficient time to cool down. Future work includes a heat management mechanism.

5. CONCLUSION AND FUTURE WORK

We modified a magnetic-filter-type plasma source to have an adjustable aperture. This modification allows for real-time control of the output (i.e., electron and ion densities) with minimal impact on the other plasma parameters. We found that, in the range of aperture opening from 4% to 100%, the plasma density changed from 0.2×10^{13} m^{-3} to 2.2×10^{13} m^{-3}. In this range, the electron temperature, plasma potential, and floating potential remained nearly constant. RPA measurements were inconclusive and the operation of the RPA needs to be investigated. Ion energies of ~10 eV were instead found using a data-fit model. Future RPA measurements are needed to corroborate the data-fit model as previously measured ion energies were ~5 eV. The settling time of the system after aperture changes as large as 10% were on the order of minutes with the majority of the settling occurring within seconds. Therefore, with this modified plasma source, ion and electron densities can be changed in a manner that would follow changes expected in a typical low Earth orbit, while the electron temperature remains nearly constant. The adjustable aperture system heats up and can bind when anode power exceeds 325 W. For future work, we intend to modify the electrical connection of the outer grid to the inner grid and provide a conductive path for heat to leave the system.

6. REFERENCES

1. Herron, B.G., Bayless, J.R. & Worden, J.D. (1973). High-voltage Solar Array Technology. *J Spacecr. Rockets*. **10**, 457–62.
2. Thiemann, H. & Bogus, K. (1986). Anomalous Current Collection and Arcing of Solar-cells Modules in a Simulated High-Density, Low-Earth-Orbit Plasma. *ESA J*. **10**, 43–57.
3. Banks, B.A., Rutledge, S.K. & Brady, J.A. (1988). The NASA Atomic Oxygen Effects Test Program. *15th Space Simulation Conf.* NASA CP-3015. Williamsburg, VA. October. 51–56.
4. Rubin, B., Farnell, C., Williams, J., Vaughn, J., Schneider, T. & Ferguson, D. (2009). Magnetic Filter Type Plasma Source for Ground-Based Simulation of Low Earth Orbit Environment. *Plasma Sources Sci. Technol*. **18**, 025015.
5. McTernan, J.K. & Bilén, S.G. (2013) The Plasma–Spacecraft Interface on Small-scale Spacecraft with Implications for Electrodynamic Tether Systems. *AIAA Space 2013 Conference*. no. 1665180, 2013.
6. Maldonado, C.A., Ketsdever, A., Rand, L.P., Xie, K., Farnell, C. & Williams, J.D. (2013). Characterization of an Atomic Oxygen Plasma Source for Ground-Based Simulation of the LEO Neutral Environment. *5th AIAA Atmospheric and Space Environments Conference*. Fluid Dynamics and Co-located Conferences, (AIAA 2013-2681).
7. Mott-Smith, H. M. & Langmuir, I. (1926). The Theory of Collectors in Gaseous Discharges. *Physical Review*. **28**, October.
8. Hutchinson, I. H. (2002). *Principles of Plasma Diagnostics*. Cambridge University Press, second edn.
9. Nichols, B. & Witteborn, F. (1966). Measurements of Resonant Charge Exchange Cross Sections in Nitrogen and Argon Between 0.5 and 17 eV. *NASA Technical Note*. TN D-3265.
10. Phelps, A.V. (1991). Cross Sections and Swarm Coefficients for Nitrogen Ions and Neutrals in N_2 and Argon Ions and Neutrals in Ar for Energies from 0.1 eV to 10 keV. *J. Phys. Chem. Ref. Data*. **20**, No. 3.
11. Sakabe, S. & Izawa, Y. (1991). Cross Sections for Resonant Charge Transfer Between Atoms and Their Positive Ions: Collision Velocity <1 a.u. *At. Data Nucl. Data Tables*. **49,** 257-314.
12. Barjatya, A., Swenson, C.M., Thompson, D.C. & Wright, K.H. (2009). Invited Article: Data analysis of the Floating Potential Measurement Unit aboard the International Space Station. *Rev. Sci. Instrum*. **80**, 041301.